ISSN 1674-1056
http://cpb.iphy.ac.cn
http://iopscience.iop.org/cpb
中国物理 B
Chinese Physics
中国物理 Chinese Physics B

Effect of Nb doping on microstructures and thermoelectric properties of $SrTiO_3$ ceramics

Da-Quan Liu(刘达权), Yu-Wei Zhang(张玉伟), Hui-Jun Kang(康慧君), Jin-Ling Li(李金玲), Xiong Yang(杨雄), Tong-Min Wang(王同敏)
Citation: Chin. Phys. B . 2018, 27(4): 047205. **doi:** 10.1088/1674-1056/27/4/047205

Journal homepage: http://cpb.iphy.ac.cn; http://iopscience.iop.org/cpb

What follows is a list of articles you may be interested in

Band engineering and precipitation enhance thermoelectric performance of SnTe with Zn-doping

Zhiyu Chen(陈志禹), Ruifeng Wang(王瑞峰), Guoyu Wang(王国玉), Xiaoyuan Zhou(周小元), Zhengshang Wang(王正上), Cong Yin(尹聪), Qing Hu(胡庆), Binqiang Zhou(周斌强), Jun Tang(唐军), Ran Ang(昂然)
Chin. Phys. B . 2018, 27(4): 047202. **doi:** 10.1088/1674-1056/27/4/047202

Se substitution and micro-nano-scale porosity enhancing thermoelectric Cu_2Te

Xiaoman Shi(史晓曼), Guoyu Wang(王国玉), Ruifeng Wang(王瑞峰), Xiaoyuan Zhou(周小元), Jingtao Xu(徐静涛), Jun Tang(唐军), Ran Ang(昂然)
Chin. Phys. B . 2018, 27(4): 047204. **doi:** 10.1088/1674-1056/27/4/047204

Enhanced thermoelectric properties of p-type polycrystalline SnSe by regulating the anisotropic crystal growth and Sn vacancy

Chengyan Liu(刘呈燕), Lei Miao(苗蕾), Xiaoyang Wang(王潇漾), Shaohai Wu(伍少海), Yanyan Zheng(郑岩岩), Ziyang Deng(邓梓阳), Yulian Chen(陈玉莲), Guiwen Wang(王桂文), Xiaoyuan Zhou(周小元)
Chin. Phys. B . 2018, 27(4): 047211. **doi:** 10.1088/1674-1056/27/4/047211

Improved thermoelectric performance in p-type $Bi_{0.48}Sb_{1.52}Te_3$ bulk material by adding $MnSb_2Se_4$

Binglei Cao(曹丙垒), Jikang Jian(简基康), Binghui Ge(葛炳辉), Shanming Li(李善明), Hao Wang(王浩), Jiao Liu(刘骄), Huaizhou Zhao(赵怀周)
Chin. Phys. B . 2017, 26(1): 017202. **doi:** 10.1088/1674-1056/26/1/017202

Unexpected low thermal conductivity and large power factor in Dirac semimetal Cd_3As_2

Cheng Zhang(张成), Tong Zhou(周通), Sihang Liang(梁斯航), Junzhi Cao(曹钧植),Xiang Yuan(袁翔), Yanwen Liu(刘彦闻), Yao Shen(沈瑶), Qisi Wang(王奇思),Jun Zhao(赵俊), Zhongqin Yang(杨中芹), Faxian Xiu(修发贤)
Chin. Phys. B . 2016, 25(1): 017202. **doi:** 10.1088/1674-1056/25/1/017202

SPECIAL TOPIC — Recent advances in thermoelectric materials and devices

Effect of Nb doping on microstructures and thermoelectric properties of $SrTiO_3$ ceramics*

Da-Quan Liu(刘达权), Yu-Wei Zhang(张玉伟), Hui-Jun Kang(康慧君)†,
Jin-Ling Li(李金玲), Xiong Yang(杨雄), and Tong-Min Wang(王同敏)

Key Laboratory of Solidification Control and Digital Preparation Technology (Liaoning Province), School of Materials Science and Engineering, Dalian University of Technology, Dalian 116024, *China*

(Received 8 January 2018; revised manuscript received 24 February 2018; published online 29 March 2018)

Nb-doped $SrTiO_3$ thermoelectric ceramics with different niobium concentrations, sintering temperatures and Sr-site vacancies are successfully prepared by high energy ball milling combined with carbon burial sintering. For fully understanding the effect of niobium doping on $SrTiO_3$, thermoelectric transport properties are systematically investigated in a temperature range from 300 K to 1100 K. The carrier mobility can be significantly enhanced, and the electrical conductivity is quadrupled, when the sintering temperature rises from 1673 K to 1773 K (beyond the eutectic temperature (1713 K) of $SrTiO_3$–TiO_2). The lattice vibration can be suppressed by the lattice distortion introduced by the doped niobium atoms. However, Sr-site vacancies compensate for the lattice distortion and increase the lattice thermal conductivity more or less. Finally, we achieve a maximum value of figure-of-merit zT of 0.21 at 1100 K for $SrTi_{0.9}Nb_{0.1}O_3$ ceramic sintered at 1773 K.

Keywords: thermoelectric materials, $SrTiO_3$, Nb-doped, sintering temperature

PACS: 72.20.Pa, 72.80.Ga, 73.50.Lw **DOI:** 10.1088/1674-1056/27/4/047205

1. Introduction

High-efficiency thermoelectric (TE) materials play a key role in energy conversion applications, relying on three thermoelectric effects named by Seebeck, Peltier, and Thomson.[1] To determine the efficiency of a thermoelectric material, the dimensionless figure-of-merit zT is introduced, which can be defined as $zT = \sigma S^2 T/\kappa$, where S, σ, T, and κ are the Seebeck coefficient, electrical conductivity, absolute temperature, and thermal conductivity, respectively. And κ is the total thermal conductivity including lattice part (κ_{ph}) and electrons part (κ_{el}). A material with a high zT requires a high power factor ($PF = \sigma S^2$) and a low thermal conductivity κ, which is difficult to achieve simultaneously due to the interactions among S, σ, and κ which are affected by carrier concentration.[2] Nanostructure, e.g. the reduction of the grain scale to nanometer, or nano-impurities, is widely employed to optimize the thermoelectric properties, especially in isotropic materials.[3,4] Small grains not only introduce more grain boundaries to scatter phonons with little effect on electrical transport but also enhance Seebeck coefficient by energy filtering effect.[5] An alternative recipe to enhance TE properties is element doping, i.e., doping rare-earth, alkali-earth, transition-metal elements, etc., which can lead to significant variations of the band structure and improvement of carrier transport properties.[6–9]

Compared with other compounds, oxide thermoelectric materials are widely investigated for their excellent high temperature stability.[10] Furthermore, oxide thermoelectric materials are usually low in cost and easy to prepare for large scale applications.[11] It has been widely demonstrated that donor doping is a powerful tool to tune the carrier concentration and mobility of an n-type $SrTiO_3$ system, especially on the Ti sites. Niobium doping on the Ti site has proved to be a successful case for enhancing $SrTiO_3$ thermoelectric properties.[12] Both Nb-doped $SrTiO_3$ epitaxial film and bulk samples have achieved a relatively high zT value of 0.37 at 1000 K by tailoring the content of niobium.[13] Besides the concentration of doping elements, the effects of sintering process and material defects on the thermoelectric transport properties of $SrTiO_3$ have attracted more attention.[14] Different sintering time and annealing temperatures have a significant influence on $SrTiO_3$ thermoelectric properties. Moreover, sintering temperature is another key factor for optimizing the electrical transport properties, especially electrical conductivity.[15] When the temperature is higher than eutectic temperature (1713 K) of $SrTiO_3$–TiO_2,[16] there may appear a liquid phase in the sintering process, which permits the ions with a larger radius to enter into $SrTiO_3$ lattice, such as Nb^{4+} or Ti^{3+} ions, and thus leading to the enhancement of electrical conductivity and the decrease of lattice thermal conductivity.[17] Introducing vacancies, either on Sr-site or on oxygen-site, has been used to

*Project supported by the National Key Research and Development Program of China (Grant No. 2017YFA0403803), the National Natural Science Foundation of China (Grant Nos. 51774065, 51525401, 51690163, and 51601028), and the Dalian Support Plan for Innovation of High-level Talents (Top and Leading Talents) (Grant No. 2015R013).

†Corresponding author. E-mail: kanghuijun@dlut.edu.cn

© 2018 Chinese Physical Society and IOP Publishing Ltd

enhance zT successfully through reducing the thermal conductivity, which can reduce thermal conductivity from $\kappa >$ 9 $W{\cdot}m^{-1}{\cdot}K^{-1}$ in pristine to 2 $W{\cdot}m^{-1}{\cdot}K^{-1}$ in defected $SrTiO_3$ bulk sample.[18,19]

In this work, we synthesize three different types of Nb-doped $SrTiO_3$ powders using high energy ball milling and sinter the powders after they have been cold-isostatic-pressed into bulk samples. The effects of sintering temperature, Nb concentration and the existence of Sr-site vacancies on the microstructure and thermoelectric property of bulk Nb-doped $SrTiO_3$ are investigated. With the increase of the sintering temperature, the electrical conductivity can be improved as a result of enhanced carrier mobility. Higher Nb content contributes to a larger lattice distortion, which suppresses the thermal conductivity. However, Sr-site vacancies compensate for the lattice distortion and increase the lattice thermal conductivity more or less. Consequently, a maximum zT value of 0.21 at 1100 K for $SrTi_{0.9}Nb_{0.1}O_3$ ceramic sintered at 1773 K can be achieved.

2. Experiment

Polycrystalline $SrTi_{0.95}Nb_{0.05}O_3$, $SrTi_{0.9}Nb_{0.10}O_3$, and $Sr_{0.95}Ti_{0.95}Nb_{0.05}O_3$ samples were prepared by high energy ball milling using SrO (Aladdin, AR), TiO_2 (Aladdin, 99%) and Nb_2O_5 (Aladdin, 99%) powders. Appropriate quantities of the raw materials were blended by hand first in a baker and then milled using a planetary mill (FRITSCH Pulverisette 4) with tungsten carbide jars and balls at a rolling speed of 200 r/min. The mass ratio was 25:1 between balls and the mixture. A milling period contained "50-min milling +10-min pause", and the whole milling time was 120 h. The as-prepared powders were pressed into disc-shaped bulk by uniaxial cold isostatic pressing. The densified samples were prepared by carbon buried sintering process in air for 5 h at different sintering temperatures. The phase composition of both powders and bulk samples was identified by x-ray diffraction (XRD, EMPYREAN diffractometer) with Cu Kα in a range of $20^\circ \leq 2\theta \leq 80^\circ$ with a sweep rate of 4° per minute. The morphologies of powders and freshly created fracture of bulk samples were characterized by field emission scanning electron microscopy equipped with an energy dispersive spectrometer (SEM/EDS, Zeiss supra 55) operated in the secondary electron mode with an accelerating voltage of 15 kV. The x-ray photoelectron spectroscopy (XPS) was carried out on polished cross-section samples using an ESCALAB 250Xi instrument with Al Kα x-ray source. Detailed scans of electronic transitions of core levels were performed with a resolution of 0.05 eV. The electrical conductivity (σ) and Seebeck coefficient (S) were simultaneously measured in a temperature range from 300 K to 1100 K in the helium atmosphere, using a commercial thermoelectric measuring system (LSR-3, Linseis Germany). Thermal diffusivity (D) was measured by a laser flash analysis (LFA 427, Netzsch). Specific heat capacity (C_p) was measured by a differential scanning calorimeter (DSC, STA 449F3, Netzsch, Germany). The thermal conductivity was calculated by multiplying the thermal diffusivity, the specific heat capacity, and geometric density (ρ) measured by the Archimedes technique, i.e., $\kappa = \rho D C_p$. The uncertainties in the Seebeck coefficient, the electrical conductivity and the thermal conductivity are estimated to be 5%, 10%, and 7%, respectively.

3. Results and discussion

Figure 1(a) shows the x-ray diffraction patterns of the $Sr_{0.95}Ti_{0.95}Nb_{0.05}O_3$, $SrTi_{0.95}Nb_{0.05}O_3$, and $SrTi_{0.9}Nb_{0.1}O_3$ powders synthesized by high energy ball milling (HEBM) with the total milling time of 120 h. After the milling process, most of the diffraction peaks can be indexed as cubic $SrTiO_3$ (PDF # 35-0734). However, some raw powders, existing as a second phase in the final product, can still be detected, and the main component is determined to be rutile TiO_2. The grain sizes of all these Nb-doped $SrTiO_3$ powders are calculated to be about 15 nm. The morphology of 5-mol% Nb-doped $SrTiO_3$ powders without A-site vacancies ($SrTi_{0.95}Nb_{0.05}O_3$) is shown in Fig. 1(b). According to the XRD results, most of the particles, each with a size of less than 1 μm, are composed of a large number of nano-grains, which is also confirmed by the high-resolution transmission electron microscopy results in our previous work.[20] Thus, HEBM can be successfully applied to the synthesis of nano-scale Nb-doped $SrTiO_3$ powders.

For easy expression, we denote $Sr_{0.95}Ti_{0.95}Nb_{0.05}O_3$, $SrTi_{0.95}Nb_{0.05}O_3$, and $SrTi_{0.9}Nb_{0.1}O_3$ powders as VNb05, Nb05, and Nb10 respectively, and add the sintering temperature to the end for bulk samples, e.g., Nb05-1773 refers to $SrTi_{0.95}Nb_{0.05}O_3$ bulk sample sintered at 1773 K. Figure 2(a) shows the XRD results of as-sintered bulk samples. The sharp diffraction peaks imply that the grains are crystallized completely and all the second phases vanish after sintering process. It means that Nb has been successfully doped into the $SrTiO_3$ lattice. The magnified (110) peaks at $2\theta = 32.4^\circ$ as shown in Fig. 2(b) indicate that each of the diffraction peaks of all the samples shifts to a lower angle with the increase of Nb content, which can be attributed to the substitution of Ti^{4+} ion (0.0605 nm) on B-site for a larger-radius Nb^{5+} ion (0.064 nm).[12] When the sintering temperature (1773 K) is beyond the eutectic temperature of $SrTiO_3$–TiO_2 (1713 K), the Nb ions can be doped into $SrTiO_3$ lattice facilely due to the existence of the liquid phase.[16,21] Because of the introduction of A-site vacancies, the lattice distortion of VNb05-1773 is compensated for to some extent. Moreover, Nb concentration, instead of the sintering temperature, has a greater influ-

ence on the lattice structure. Thus the angle of (110) diffraction peak is in the order of VNb05-1773>Nb05-1673 = Nb05-1773>Nb10-1773. The relative densities of the four samples, Nb05-11673, Nb05-1773, VNb05-1773, and Nb10-1773, are 89.8%, 92.8%, 91.0%, and 93.8%, respectively.

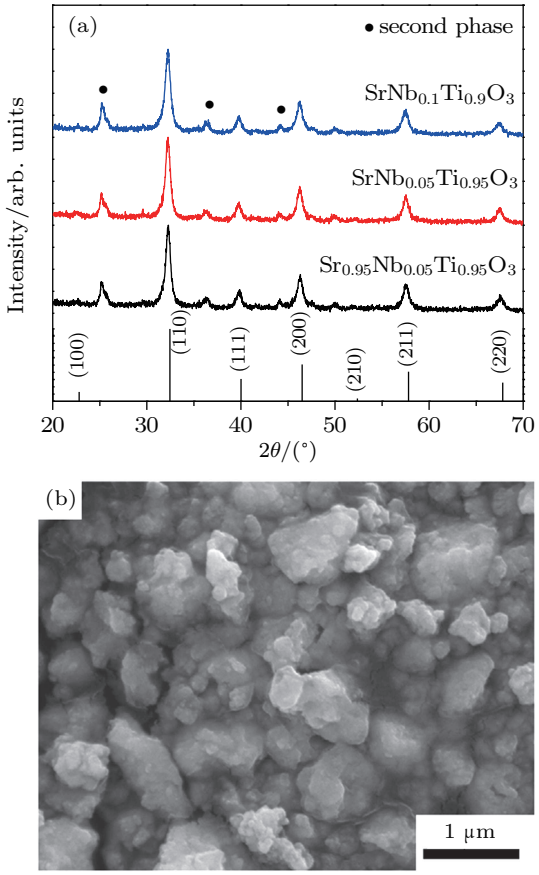


Fig. 1. (color online) Powder structure characterization after 120-h milling: (a) XRD patterns for $Sr_{0.95}Ti_{0.95}Nb_{0.05}O_3$, $SrTi_{0.95}Nb_{0.05}O_3$, and $SrTi_{0.9}Nb_{0.1}O_3$ powders; (b) SEM image of $SrTi_{0.95}Nb_{0.05}O_3$ powders.

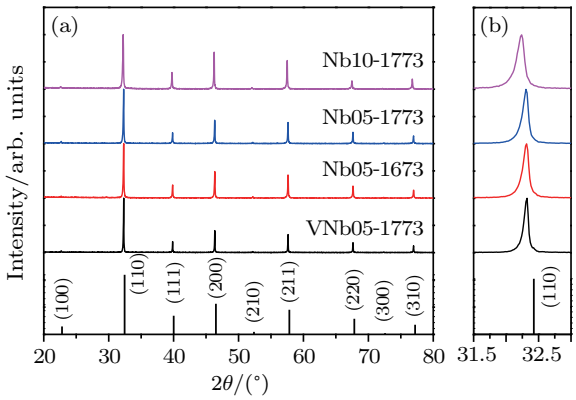


Fig. 2. (color online) XRD patterns of sintered Nb-doped samples (a) $20° \le 2\theta \le 80°$, (b) $31.5° \le 2\theta \le 33°$, with magnifying (110) peak.

The SEM images of the freshly created fractures for bulk samples indicate quite similar surface morphologies as shown in Fig. 3. The grain sizes of all four sintered samples are in a range of 2 μm–3 μm. In Fig. 3(a), there are some pores in the matrix of Nb05-1673 sample, which is in accord with the lowest relative density. When the sintering temperature increases to 1773 K, the better sintering quality enhances the relative density of Nb05-1773 bulk sample. The VNb05-1773 sample has a more uniform grain size than other sintered samples, because the presence of strontium vacancies has promoted the solid-state diffusion process.[14] On the other hand, according to the bulk XRD patterns in Fig. 2(b), the introduction of A-site vacancies can reduce lattice distortion caused by the Nb-doping. When the Nb content increases to 10 mol%, the larger lattice distortion will suppress the grain growth in the sintering process,[22] and the smallest grain size can be obtained among the four sintered bulk samples, corresponding to the highest relative density.

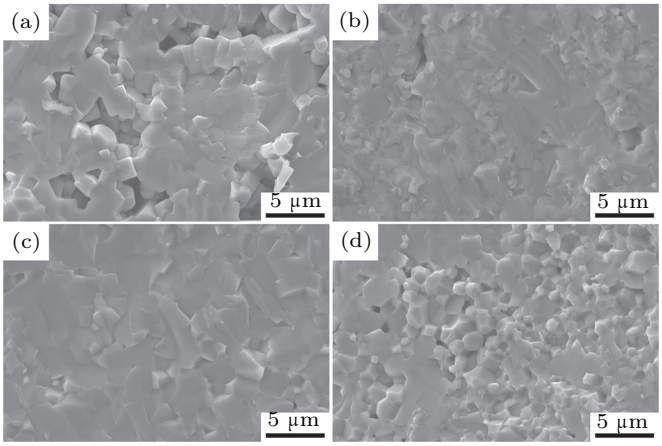


Fig. 3. (color online) SEM images of freshly broken surface of (a) $SrTi_{0.95}Nb_{0.05}O_3$ sintered at 1673 K (Nb05-1673), (b) $SrTi_{0.95}Nb_{0.05}O_3$ sintered at 1773 K (Nb05-1773), (c) $Sr_{0.95}Ti_{0.95}Nb_{0.05}O_3$ sintered at 1773 K (VNb05-1773), and (d) $SrTi_{0.9}Nb_{0.1}O_3$ sintered at 1773 K (Nb10-1773).

To understand the transport properties of charge carriers, it is essential to know about the redox states of the metal cations in the Nb-doped $SrTiO_3$ bulk samples. The defect reaction equation is shown as follows (the reaction of stoichiometric $SrTi_{0.95}Nb_{0.05}O_{3\pm\delta}$ is taken for example):[14]

$$\begin{aligned} &SrO + 0.025Nb_2O_5 + 0.95TiO_2 \rightarrow \\ &Sr_{Sr}^{\times} + 0.05Nb_{Ti}^{\bullet} + (0.9-2\delta)Ti_{Ti}^{\times} + (0.05+2\delta)Ti'_{Ti} + \delta V_O^{\bullet\bullet} \\ &\quad + (3-\delta)O_O^{\times} + (0.0125-\delta/2)O_2. \end{aligned} \tag{1}$$

The x-ray photoelectron spectroscopy (XPS) was used to identify the chemical electronic states of Nb and Ti cations for reduced $SrTi_{0.95}Nb_{0.05}O_{3\pm\delta}$ sintered at 1773 K (Nb05-1773). The XPS spectra of Ti 2p and Nb 3d are shown in Fig. 4, and the fitting lines are marked with dash lines. The high-resolution Ti 2p spectrum (Fig. 4(a)) comprises two $2p_{3/2}$ and $2p_{1/2}$ spin–orbit doublets. The main doublet with banding energies of 458.5 eV/464.3 eV is attributed to Ti^{4+} cations.[23] And the weak band, shifted to the lower banding energy (457.8 eV), is characteristic for the contribution from Ti^{3+} cations.[24] The Nb 3d spectrum (Fig. 4(b)) spits into two main lines at 207.1 eV/209.8 eV, corresponding to $3d_{5/2}$ and $3d_{3/2}$ core levels, respectively. Under the high spectrum resolution,

two additional weak peaks are detected at 205.7 eV/209.1 eV, representing a fingerprint of Nb^{4+} cations.[14,22] The relative concentrations of $Ti^{3+}$and Nb^{4+} cations calculated from the peak areas are 36% and 11%, respectively. Comparing with the reported data,[22] such a high reduced Ti^{3+} cation content results from the existence of the liquid phase in the sintering process, which has a great effect on the carrier transportation.

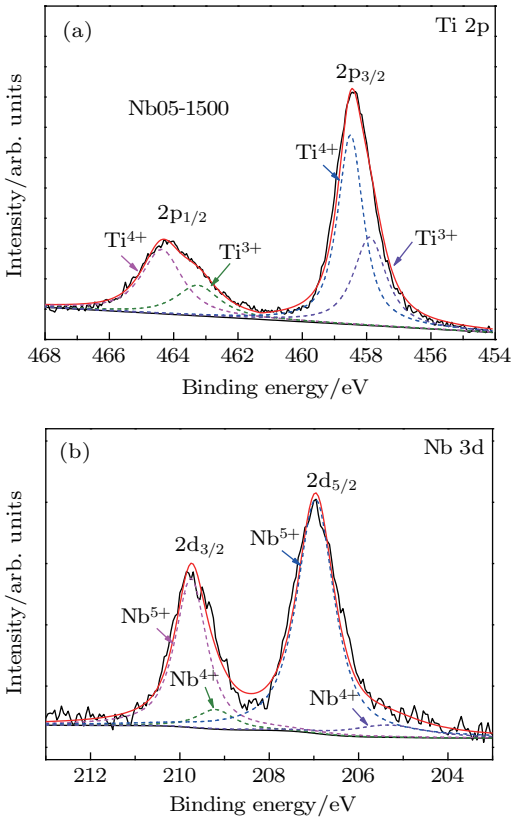


Fig. 4. (color online) High-resolution XPS spectra of (a) Ti 2p and (b) Nb 3d core-level regions, showing the corresponding fit for $SrTi_{0.95}Nb_{0.05}O_{3\pm\delta}$ ceramics sintered at 1773 K (Nb05-1773).

The temperature-dependent electrical transport properties for these carbon burial sintered Nb-doped $SrTiO_3$ samples are systematically investigated in a temperature range from 300 K to 1100 K as shown in Fig. 5. The Seebeck coefficient can be expressed as

$$S = \frac{8\pi^2 k_B^2}{3eh^2} m^* T \left(\frac{\pi}{3n}\right)^{2/3}, \tag{2}$$

where k_B, e, h, n, and m^* are the Boltzmann constant, electron charge, Planck constant, carrier concentration, and effective mass of carrier, respectively. The electrical conductivity (σ) is related to the carrier concentration n and carrier mobility μ, that is,[25]

$$\sigma = ne\mu. \tag{3}$$

The negative Seebeck coefficients of all samples represent an n-type electrical transport behavior (Fig. 5(a)). The 5%-mol Nb-doped samples, including Nb05-1673, Nb05-1773, and VNb05-1773 samples, can be considered to have the similar band structures and m^* values. The Nb05-1673 and VNb05-1773 samples almost have the same Seebeck coefficient, and the absolute value differences ($|\Delta S|$) between Nb05-1673 (-152.8 μV/K~ -258.1 μV/K) and Nb05-1773 (-133.1 μV/K~ -237.4 μV/K) samples are about 20 μV/K in the whole measuring temperature range. According to formula (2), we can estimate the enhancement of carrier concentration at about 1.24 times caused by the increase of sintering temperature. Actually, the extrinsic carrier concentration is usually temperature independent and determined by the doping concentration.[26] As shown in Fig. 5(b), the electrical conductivity $\sigma(T)$ of Nb05-1773 is approximately twice that of Nb05-1673. From formula (3), it is obvious that higher sintering temperature can improve carrier mobility significantly, and this result is also observed in Ref. [15]. The main reason for the enhancement may be due to the existence of the liquid phase when the temperature is higher than eutectic temperature of $SrTiO_3$–TiO_2. Comparing with Nb05-1773 sample, the existence of Sr-site vacancies in VNb05-1773 may introduce electron to be trapped and cause the carrier mobility to deteriorate. The $\sigma(T)$ values of 5-mol% Nb-doped $SrTiO_3$ show a similar trend in the whole measuring temperature range and attain peak values at around 450 K, corresponding to the thermally excited excess electrons from the reduced metallic cations. Although m^* increases with the increase of Nb content,[27] the increase of the carrier concentration plays a dominant role in the declining of Seebeck coefficient for Nb10-1773 sample. The electrical conductivity of Nb10-1773 declines from 1150 S/cm to 162 S/cm with the increase of temperature, which shows a typical metallic behavior. The relationship between σ and T can be fitted by a relation that σ is proportional to $T^{-0.9}$, $T^{-1.05}$, $T^{-1.3}$ for Nb05-1673, VNb05-1773, and Nb05-1773 samples when the temperature beyond 500 K, respectively, and σ is proportional to $T^{-1.8}$ for Nb10-1773 sample in the whole measuring temperature range, suggesting that the phonon scattering is a dominant mechanism and becomes distinct with the increase of the electrical conductivity.[21]

According to the Seebeck coefficient and electrical conductivity, the calculated power factor ($PF = S^2\sigma$) is shown in Fig. 5(c). The values of PF initial increase with the increase of temperature until 620 K for 5%-mol Nb-doped $SrTiO_3$ samples and 470 K for 10%-mol Nb-doped and decrease thereafter. The temperature for the peak value of PF is approximately 100 K higher than that of σ, due to the rapid increase of absolute $|S|$ value before 700 K. The Nb10-1773 exhibits a maximum power factor of ~ 0.99 mW·m^{-1}·K^{-2} at 472 K and then declines to ~ 0.6 mW·m^{-1}·K^{-2} at 1100 K.

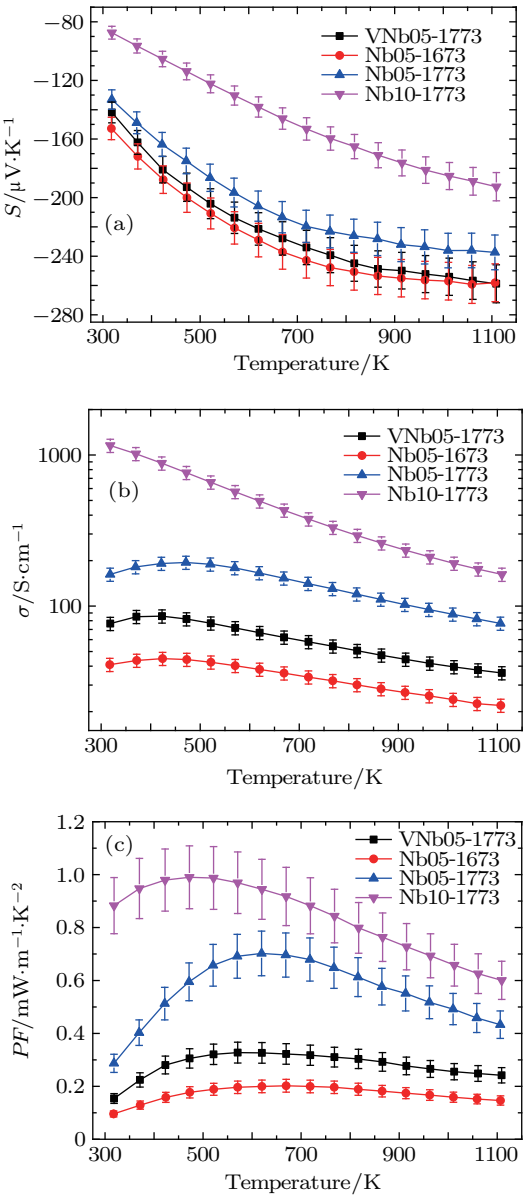


Fig. 5. (color online) Temperature-dependent (a) Seebeck coefficients, (b) electrical conductivities, and (c) power factors for the sintered Nb-doped $SrTiO_3$ samples.

The temperature-dependent total thermal conductivities is shown in Fig. 6(a), in which electron transportation and lattice vibration dominate, described as $\kappa_{tot} = \kappa_{el} + \kappa_{ph}$, where κ_{el} and κ_{ph} are electronic thermal conductivity and lattice thermal conductivity, respectively. The total thermal conductivity for all samples decreases from 7.5 $W{\cdot}m^{-1}{\cdot}K^{-1}$ to 2.5 $W{\cdot}m^{-1}{\cdot}K^{-1}$ with the increase of the temperature. The κ_{tot} values of all samples for the sintering temperature at 1773 K are almost the same, and the sample of Nb05-1673 has a lower κ_{tot} in the whole measuring temperature range. The electronic part satisfies the Wiedemann–Franz law $\kappa_{el} = \sigma LT$, where L (2.44×10^{-8} $V^2{\cdot}K^{-2}$) is the Lorenz number.[21] As it is hard to realize high σ and low κ_{el} simultaneously, the lattice thermal conductivity (κ_{ph}) always plays a dominant role in total thermal conductivity and the strategy to reduce κ_{ph} is the key point for high figure-of-merit zT. Figure 6(b) shows the temperature dependence of κ_{ph} for different samples. The Nb10-1773 sample has the minimum κ_{ph} values from 300 K to 850 K, and Nb05-1673 has the lowest κ_{ph} values when temperature is higher than 850 K. In this study, due to the similar grain sizes for all samples, the lattice vibrations (phonons) are the major factor considered for thermal transportation, and the contribution of grain boundary scattering can be ignored. From the XRD patterns of bulk samples, the greater peak angle shift corresponds to a lower κ_{ph}. This is a powerful evidence that larger lattice distortion may suppress the lattice vibration and thus reduce the lattice thermal conductivity. However, there exists an abnormal increase in lattice conductivity for Nb10-1773 sample. The main reason can be that the carrier concentration of the sample is far higher than other concentrations, and the carrier vibration will exert more effect on the lattice especially at a high temperature. Based on the previous analysis, it can be concluded that the increase of the sintering temperature has not an obvious effect on thermal conductivity, especially in a high temperature range.

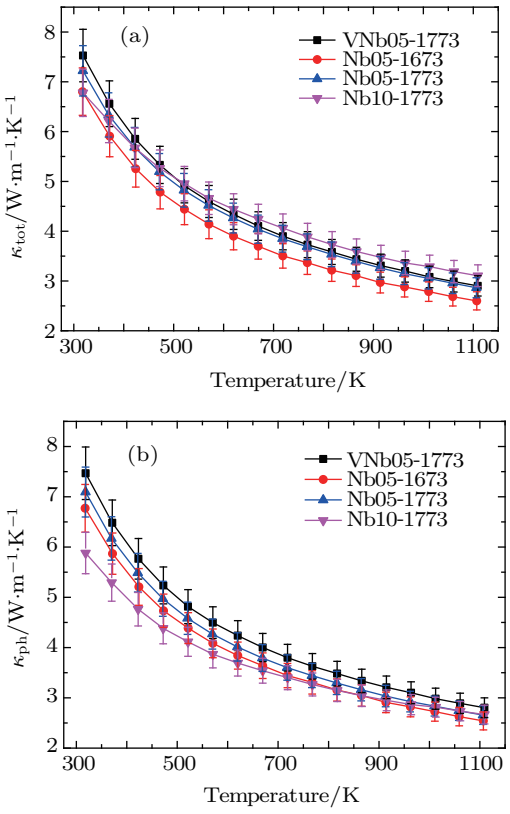


Fig. 6. (color online) Temperature dependence of (a) total and (b) lattice thermal conductivity for the sintered Nb-doped $SrTiO_3$ samples.

By integrating the electrical and thermal transport properties discussed above, the temperature-dependent dimensionless figure-of-merit zT values are shown in Fig. 7. All curves increase monotonically with the increase of temperature, and the maximum values of 0.09, 0.06, 0.17, and 0.21 at 1100 K for VNb05-1773, Nb05-1673, Nb05-1773, and Nb10-1773

bulk samples can be achieved, respectively. Because there is no obvious difference in thermal conductivity among these samples at high temperature which is the proper working temperature for the TE application of $SrTiO_3$ ceramics, the core of high zT value for the future study is used to balance the Seebeck coefficient and electrical conductivity, i.e., to obtain a high power factor.

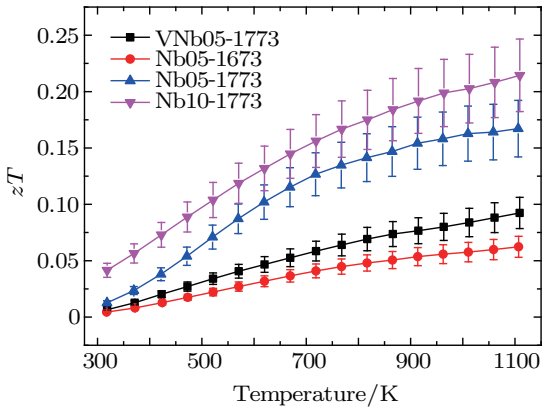


Fig. 7. (color online) Temperature-dependent dimensionless figure-of-merit zT values for the sintered Nb-doped $SrTiO_3$ samples.

4. Conclusions

In this paper, Nb-doped $SrTiO_3$ ceramic has been successfully prepared by high energy ball milling combined with carbon burial sintering. Thermoelectric transport properties of bulk $SrTiO_3$ samples with different Nb concentrations, sintering temperatures and Sr-site vacancies are systematically investigated. And we can draw the conclusions as follows. (i) Doped niobium atom can enhance lattice distortion and suppress the lattice vibration, which has a dominant effect on reducing lattice thermal conductivity. (ii) The sintering temperature, higher than eutectic point of $SrTiO_3$–TiO_2, can significantly improve the carrier mobility and thus the electrical conductivity. (iii) The introducing of Sr-site vacancies can depress the figure-of-merit zT, as a consequence of high thermal conductivity and low carrier mobility caused by compensating for lattice distortion and suppressing the electron trap. A maximum zT value of 0.21 at 1100 K for $SrTi_{0.9}Nb_{0.1}O_3$ ceramic sintered at 1773 K can be achieved.

References

[1] He J and Tritt T M 2017 *Science* **357** 1369
[2] Snyder G J and Toberer E S 2008 *Nat. Mater.* **7** 105
[3] Koumoto K, Wang Y, Zhang R, Kosuga A and Funahashi R 2010 *Ann. Rev. Mater. Res.* **40** 363
[4] Wang J, Ye X X, Yaer X B, Zhang B Y, Ma W and Miao L 2015 *Scr. Mater.* **99** 25
[5] Wang Y F, Zhang X Y, Shen L M, Bao N Z, Wan C L, Park N H, Koumoto K and Gupta A 2013 *J. Power Sources* **241** 255
[6] Sootsman J R, Chung D Y and Kanatzidis M G 2009 *Angew. Chem. Int. Edit.* **48** 8616
[7] Liu Y, Cadavid D, Ibáñez M, Ortega S, Martí-Sánchez S, Dobrozhan O, Kovalenko M V, Arbiol J and Cabot A 2016 *APL Mater.* **4** 104813
[8] Cui Y J, Salvador J R, Yang J H, Wang H, Amow G and Kleinke H 2009 *J. Electron. Mater.* **38** 1002
[9] Zhang Y C, Liu J, Li Y, Chen Y F, Li J C, Su W B, Zhou Y C, Zhai J Z, Wang T and Wang C L 2017 *Chin. Phys. B* **26** 107201
[10] Koumoto K, Terasaki I and Funahashi R 2006 *Mrs. Bull.* **31** 206
[11] Fergus J W 2012 *J. Eur. Ceram. Soc.* **32** 525
[12] Zhang B Y, Wang J, Zou T, Zhang S, Yaer X B, Ding N, Liu C Y, Miao L, Lia Y and Wua Y 2015 *J. Mater. Chem. C* **3** 11406
[13] Ohta S, Nomura T, Ohta H, Hirano M, Hosono H and Koumoto K 2005 *Appl. Phys. Lett.* **87** 092108
[14] Kovalevsky A V, Aguirre M H, Populoh S, Patricio S G, Ferreira N M, Mikhalev S M, Fagg D P, Weidenkaff A and Frade J R 2017 *J. Mater. Chem. A* **5** 3909
[15] Li L L, Qin X Y, Liu Y F and Liu Q Z 2015 *Chin. Phys. B* **24** 067202
[16] Cocco A and Massazza F 1963 *Ann. Chim-rome.* **53** 883
[17] Il Kim S, Lee K H, Mun H A, Kim H S, Hwang S W, Roh J W, Yang D J, Shin W H, Li X S, Lee Y H, Snyder G J and Kim S W 2015 *Science* **348** 109
[18] Han J, Sun Q and Song Y 2017 *J. Alloys Compd.* **705** 22
[19] Liu J, Wang C L, Su W B, Wang H C, Zheng P, Li J C, Zhang J L and Mei L M 2009 *Appl. Phys. Lett.* **95** 162110
[20] Liu D Q, Zhang Y W, Kang H J, Li J L, Chen Z N and Wang T M 2018 *J. Eur. Ceram. Soc.* **38** 807
[21] Park K, Son J S, Woo S I, Shin K, Oh M W, Park S D and Hyeon T 2014 *J. Mater. Chem. A* **2** 4217
[22] Srivastava D, Norman C, Azough F, Schafer M C, Guilmeau E, Kepaptsoglou D, Ramasse Q M, Nicotra G and Freer R 2016 *Phys. Chem. Chem. Phys.* **18** 26475
[23] Werfel F and Brümmer O 1983 *Phys. Scr.* **28** 92
[24] Hu Y, Tan O K, Pan J S and Yao X 2004 *J. Phys. Chem. B* **108** 11214
[25] Tan G, Zhao L D and Kanatzidis M G 2016 *Chem. Rev.* **116** 12123
[26] Pei Y Z, Heinz N A and Snyder G J 2011 *J. Mater. Chem.* **21** 18256
[27] Wunderlich W, Ohta H and Koumoto K 2009 *Physica B* **404** 2202